Research Square

Preprints are preliminary reports that have not undergone peer review.
They should not be considered conclusive, used to inform clinical practice,
or referenced by the media as validated information.

Effects of multivariate recovery dependency on resilience and scaling laws in networks with time delays

Xun Zhou
Jiangsu University
Fan Wang
Nanjing Normal University
Ruijin Du
mathdudo@ujs.edu.cn

Jiangsu University
Duxin Chen
chendx@seu.edu.cn

Southeast University
Hillel Sanhedrai
Bar-Ilan University
Renaud Lambiotte
University of Oxford
Gaogao Dong
gago999@126.com

Jiangsu University

Research Article

Keywords: complex systems, complex network modeling, network repair, multilayer networks, cross-scale coupling

Posted Date: November 25th, 2026

DOI: https://doi.org/10.21203/rs.3.rs-7107176/v2

License: This work is licensed under a Creative Commons Attribution 4.0 International License.
Read Full License

Additional Declarations: The authors declare no competing interests.

Effects of multivariate recovery dependency on resilience and scaling laws in networks with time delays

Xun Zhou,[1,*] Fan Wang,[2,*] Ruijin Du,[1,†] Duxin Chen,[3,‡]
Hillel Sanhedrai,[4] Renaud Lambiotte,[1,5] and Gaogao Dong[1,2,§]

[1]*School of Mathematical Sciences, Jiangsu University, Zhenjiang 212013, China*

[2]*Ministry of Education Key Laboratory of NSLSCS,*
School of Mathematical Sciences, Nanjing Normal University, Nanjing 210023, China

[3]*School of Mathematics, Southeast University, Nanjing 211189, China*

[4]*Department of Physics, Bar-Ilan University, Ramat-Gan 52900, Israel*

[5]*Mathematical Institute, University of Oxford, Oxford OX2 6GG, UK*

Abstract

Real-world recovery processes in interdependent systems are rarely instantaneous and often involve time delays, yet their impact on network-level resilience remains poorly understood. We propose a dynamical recovery model on interdependent networks in which node-level recovery depends on both intra-layer and inter-layer support and is activated only after a finite delay. Combining mean-field analysis with large-scale simulations, we examine the long-term recovery outcomes under varying levels of initial damage and recovery delays. We identify two distinct recovery thresholds that partition the system into *fully recoverable*, *partially recoverable*, and *unrecoverable* regimes, corresponding to different basins of attraction in the recovery dynamics. While increasing recovery delays substantially reduces both the probability and the speed of successful recovery, the ultimate collapse threshold is governed primarily by network structure. In contrast, the lower recovery threshold is sensitive to both network size and recovery delay, whereas the upper threshold remains robust to these factors. As a result, the separation between the two thresholds follows a scaling law with network size and increases linearly with the recovery delay. Our results highlight the critical role of timely interventions in enhancing resilience and provide insights for designing recovery strategies in coupled infrastructures.

Keywords: complex systems, complex network modeling, network repair, multilayer networks, cross-scale coupling

*These authors contributed equally to this work.
†Corresponding author: mathdudo@ujs.edu.cn
‡Corresponding author: chendx@seu.edu.cn
§Corresponding author: gago999@126.com

I. INTRODUCTION

Complex systems' resilience is vital for maintaining the stability and functionality of networked systems when failures or errors occur [1–11]. Failures within these networks often arise from a combination of endogenous factors, such as internal component malfunctions, and exogenous factors, such as natural disasters or cyberattacks [12–18]. This dual nature of failure presents a challenge to effectively maintaining system resilience.

As the coupling and dependence among systems increase, local failures, if not promptly repaired, may lead to catastrophic collapse [19–24]. Preventing network collapse by strengthening the network topology, such as node or link addition, or increasing link strengths, is an important way to enhance the resilience of complex networked systems [25–29]. A more direct question for a functionally impaired network is whether and how it can recover. The recovery process is dynamic, influenced by factors such as the scale of initial damage and network topology. Timely and effective recovery strategies are crucial for restoring system resilience and maintaining operational capability [30–33]. Faults arise from both endogenous and exogenous factors, each of which affects recovery behavior through different mechanisms. Consequently, the restoration of the system's overall functionality necessitates coordinated internal and external recovery efforts, as failures—whether internal or external to the network—can significantly hinder the recovery process and undermine the overall effectiveness of the system's response [34–36].

Recovery from multiple failures has been examined from various perspectives. Majdandzic et al. [33] proposed a spontaneous recovery model for nodes experiencing multiple failures, where each node alternately switches between high and low states, resulting in the macroscopic emergence of phase-flipping behavior. Liu et al. [37] analyzed internal and external failures in directed networks, revealing that networks with Markovian recovery maintain a higher level of activity than those with non-Markovian recovery. Peng et al. [38] investigated multiple failures in higher-order networks and found that heterogeneous hypergraphs exhibited greater resilience during the recovery process. Daniotti et al. [39] demonstrated that diverse failure types can markedly increase the risk of cascading failures and proposed a strategy to mitigate these effects. A recent study [40] has shown that, in certain scenarios, node recovery depends on the state of an external support network, a process known as external dynamic repair. Such cross-system recovery support can be bidirectional. In real-world infrastructure systems, different systems may provide essential functional support to each other during recovery. For example, the restoration of transportation facilities requires power supply, while the repair of power facilities depends on road accessibility [41]. Similarly, the

recovery of interdependent power and gas distribution systems requires coordinated allocation of emergency supply and repair resources [42]. In other cases, however, simultaneous internal failures may occur within the network, necessitating internal repair, which is influenced by the network's intrinsic structural state.

The timing of recovery interventions is another crucial factor to consider [43–45]. In the real world, immediate recovery is rare, as delays often arise due to logistical constraints, limited conditions, or physical distance between affected nodes [40, 46, 47]. These delays can significantly hinder recovery, increasing the risk of cascading failures and prolonging system outages. The time delay, denoted as τ, plays a critical role in recovery dynamics, representing the interval between the initial attack and the initiation of recovery actions.

In this study, we aim to explore the dependencies on both internal and external factors during network recovery, a concept we refer to as multivariate recovery dependency. Time delays, another crucial factor influencing recovery dynamics, are also incorporated into our model. A central feature of our model is that once recovery interventions begin, each node has a time-varying recovery rate determined by both intra-layer (internal) and inter-layer (external) dependencies. Unlike existing recovery models that rely purely on spontaneous internal rates or purely on external dynamic repair, we propose a mechanism in which the recovery of a failed node is simultaneously dictated by the real-time functional state of both its local neighborhood and its external-support counterpart. This dynamic, cross-layer coupling of micro-local states captures the indispensable nature of dual resources in real-world repairs. We measure the success of network recovery by the stabilized proportion of functional nodes. Furthermore, via independent numerical simulations, we define the probability of recovery success. This allows us to characterize the relationship between recovery dynamics and network structure from a macroscopic perspective. By examining the role of multivariate recovery dependency in network resilience, this study enhances the understanding of recovery dynamics in interdependent networks and offers practical insights for strengthening the resilience of real-world systems.

II. MODEL FRAMEWORK AND ANALYTICAL APPROACH

A. Network structure and failure-recovery processes

Our model is based on an interdependent network with a one-to-one correspondence between networks X and Y, each containing an identical number of nodes, N, as shown in Figure 1(a).

The nodes in the two layers are distinct, with corresponding nodes assigned the same index. In this study, X is referred to as the self-layer for simplicity, while Y is designated as the external-support layer. We assign states $x_i(t)$ and $y_i(t)$ to each node in layers X and Y, respectively, where a value of 1 or 0 indicates whether the node is functional or nonfunctional. The dynamic evolution of these states is modeled through discrete time steps $t = 0, 1, 2, \cdots$. Assuming all nodes are initially fully functional, node failures occur in a two-stage process. Step I. At $t = 0$, a fraction p of nodes in each layer fail. Step II. For $t > 0$, each functional node in layer μ is subject to a failure rate γ_μ^{d} at each time step. These two stages of failure respectively represent an initial attack and subsequent random failures. Although immediate recovery following a failure is ideal, it is often unattainable in practical scenarios, such as geological disasters, limited availability of recovery vehicles, or the remoteness of affected areas. To capture this effect, we incorporate a recovery delay τ, during which failed nodes cannot be restored. Figure 1(b) illustrates this multivariate recovery dependency during the recovery process. When node i in the self-layer X fails, its recovery depends on its neighbors in the self-layer, as well as on its corresponding node in the external-support layer Y and that node's neighbors. Multivariate recovery dependency is observed in real-world systems. For instance, in an interdependent system consisting of both road and power networks, restoring failed components of the road network necessitates access to transportation, which is provided by the self-layer, as well as the use of electrical equipment, which relies on the external-support layer. Figure 1(c) illustrates the dynamic evolution of the system under failure and recovery. During the interval $0 < t < \tau$, recovery remains inactive while random failures continue to occur, causing damage to accumulate in the system. For $t \geq \tau$, recovery and random failures proceed concurrently, with the recovery process depending jointly on the functional states of the self-layer and the external-support layer.

B. Modeling multivariate recovery dependency with time delays

The baseline recovery rate of each node in layer μ is defined as

$$\gamma_\mu^{\mathrm{r},0} = \gamma_{\mu,\mathrm{inner}}^{\mathrm{r},0} \gamma_{\mu,\mathrm{inter}}^{\mathrm{r},0}, \tag{1}$$

where $\gamma_{\mu,\mathrm{inner}}^{\mathrm{r},0}$ and $\gamma_{\mu,\mathrm{inter}}^{\mathrm{r},0}$ represent the baseline recovery contributions obtained from the self-layer and the external-support layer, respectively. The constant $\gamma_\mu^{\mathrm{r},0}$ represents a fixed level of recovery. In our model, building on the approach of Ref. [40], we go beyond the simple setting by considering cases where the baseline recovery is modulated by the states of the respective network, causing

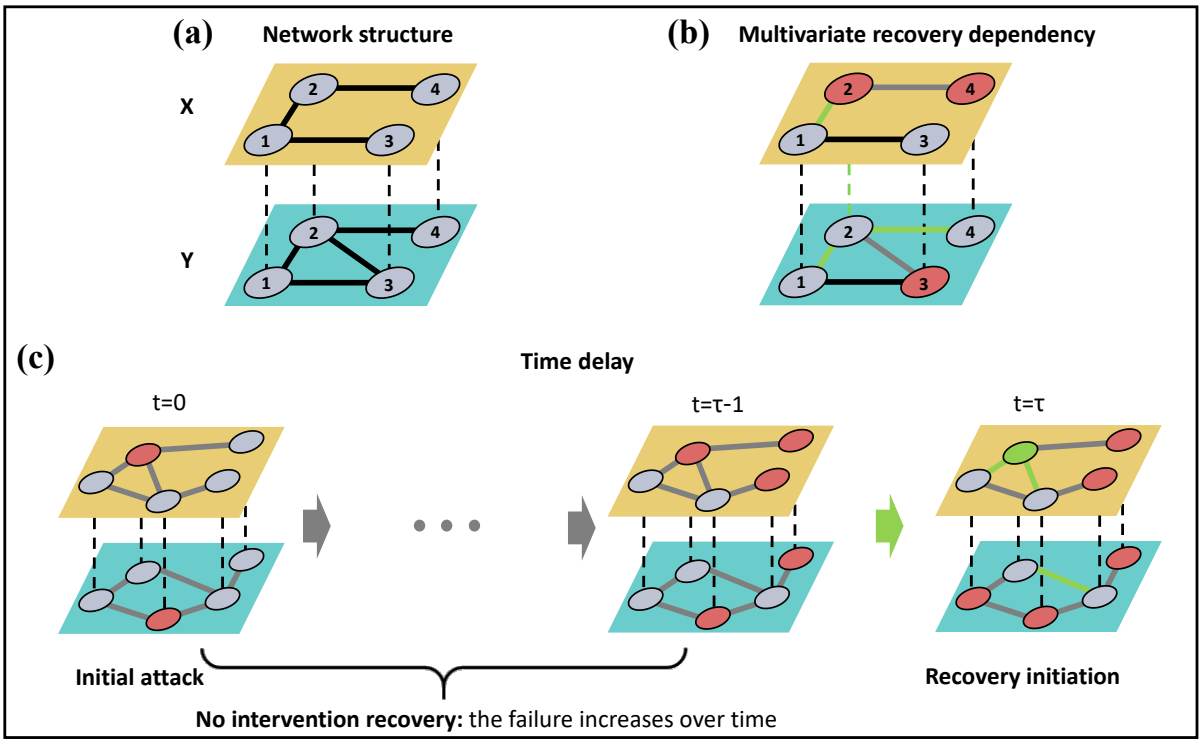

FIG. 1: Schematic diagram of failure and recovery in interdependent networks. (a) Demonstration of the network structure. Solid black lines represent intra-layer links within each network, while dashed black lines represent inter-layer links connecting nodes in layers X and Y. (b) When node 2 in layer X is disabled (red node), a recovery process is initiated. Nodes 1 and 4 in layer X, along with nodes 1, 2, 3 and 4 in layer Y, provide support to node 2 in layer X (green solid lines). However, some support nodes are also in a failed state, leading to interruptions in support links (grey solid lines). (c) Dynamic evolution of the network system under time delay. The recovery process remains inactive during the delay interval and is initiated at $t = \tau$.

the actual recovery rate of nodes to vary over time. We define the time-dependent recovery rate $\gamma^{\mathrm{r}}_{X,i}(t)$ of node i by incorporating time delays in layer X as

$$\gamma^{\mathrm{r}}_{X,i}(t) = \begin{cases} 0 & t < \tau \\ \gamma^{\mathrm{r},0}_{X,\mathrm{inner}} \gamma^{\mathrm{r},0}_{X,\mathrm{inter}} \varphi(\langle x_i(t) \rangle) \psi(\langle y_i(t) \rangle) & t \geq \tau \end{cases}. \tag{2}$$

In (2), recovery remains inactive before the delay τ and becomes active once this delay has elapsed. In fact, the recovery support associated with layers X and Y may have different time delays, denoted by τ_X and τ_Y, respectively. Yet because node recovery requires support from both network layers, the effective recovery delay is determined by the support that becomes available later, i.e., $\tau = \max(\tau_X, \tau_Y)$. The functions $\varphi(x)$ and $\psi(x)$ capture the internal and external recovery

dependencies around node i on layers X and Y, respectively. Here, we define $\varphi(x)$ and $\psi(x)$ as

$$\varphi(\langle x_i(t)\rangle) = 1 - \alpha_1(1 - \langle x_i(t)\rangle), \tag{3}$$

and

$$\psi(\langle y_i(t)\rangle) = 1 - \alpha_2(1 - \langle y_i(t)\rangle), \tag{4}$$

where $\alpha_j \in [0, 1]$ $(j = 1, 2)$ represents the interaction strength, reflecting the extent to which the self-layer X $(j = 1)$ or the external-support layer Y $(j = 2)$ affects the recovery process. The forms of (3) and (4) are derived via linearization, with the detailed derivation provided in Appendix B of the Supplementary Material. Here, we combine the two dependency functions multiplicatively to represent a coupled constraint. This formulation captures the joint influence of internal and external support on node recovery. Specifically, a reduction in either internal or external support decreases the overall recovery rate, indicating that the recovery rate is jointly constrained by both sources of support. When $\alpha_j = 1$, the recovery process is entirely dependent on the self-layer $(j = 1)$ or the external-support layer $(j = 2)$. Conversely, when $\alpha_j = 0$, the recovery process is completely independent of the corresponding network layer. The average state of node i is expressed as

$$\langle x_i(t)\rangle = \frac{1}{k_{X,i}} \sum_j X_{ij} x_j(t), \tag{5}$$

and

$$\langle y_i(t)\rangle = \frac{1}{k_{Y,i} + 1} \sum_j \widetilde{Y}_{ij} y_j(t), \tag{6}$$

where X_{ij} and $\widetilde{Y}_{ij}$ are the adjacency matrices of the corresponding networks, and $k_{X,i}$ and $k_{Y,i}$ denote the degrees of node i in layers X and Y, respectively. These two quantities capture the evolving local state around node i in layer X and its recovery-dependent node in layer Y, respectively, indicating that the recovery resources are sourced from the vicinity of the failure. Note that in (6), we use $\widetilde{Y}_{ij} = Y_{ij} + I_{ij}$ instead of Y_{ij}, where I_{ij} represents the element of the identity matrix. This construction ensures that, for a failure occurring in network X, the corresponding interdependent nodes are included among the recovery support nodes. For network Y, the recovery rate $\gamma^{\mathrm{r}}_{Y,i}(t)$ is defined analogously to that of network X.

C. Evolution and steady state

Assuming a global recovery rate $\gamma_\mu^{\mathrm{r}}(t)$, the evolution of the functional fraction f_μ is given by

$$f_\mu(t+1) = f_\mu(t) + \gamma_\mu^{\mathrm{r}}(t)(1 - f_\mu(t)) - \gamma_\mu^{\mathrm{d}} f_\mu(t), \tag{7}$$

where γ_μ^{d} denotes the failure rate in layer μ at each time step. The initial condition is $f_\mu(0) = 1-p$. When $t < \tau$, $\gamma_\mu^{\mathrm{r}}(t) = 0$, and (7) gives the solution $f_\mu(t) = (1-\gamma_\mu^{\mathrm{d}})^t(1-p) \approx (1-p)\mathrm{e}^{-\gamma_\mu^{\mathrm{d}} t}$ (see Appendix C of the Supplementary Material for further details). This transforms (7) into

$$\begin{cases} f_\mu(t) = (1-p)\mathrm{e}^{-\gamma_\mu^{\mathrm{d}} t} & t < \tau \\ f_\mu(t+1) - f_\mu(t) = \gamma_\mu^{\mathrm{r}}(t)(1 - f_\mu(t)) - \gamma_\mu^{\mathrm{d}} f_\mu(t) & t \geq \tau \end{cases}. \tag{8}$$

For $t \geq \tau$, setting the left-hand side of (8) to zero yields

$$0 = \gamma_\mu^{\mathrm{r},*}(1 - f_\mu^*) - f_\mu^* \gamma_\mu^{\mathrm{d}}, \tag{9}$$

where $\gamma_\mu^{\mathrm{r},*}$ and f_μ^* represent the equilibrium recovery rate and functional fraction, respectively, when the system converges ($t \to \infty$). In this equilibrium state, solving for f_μ^* gives

$$f_\mu^* = \frac{1}{1 + \frac{\gamma_\mu^{\mathrm{d}}}{\gamma_\mu^{\mathrm{r},*}}}. \tag{10}$$

When the system is in equilibrium, all nodes can be treated as homogeneous according to percolation theory [48, 49]. Thus, we can analytically derive the approximation of the local average state of the nodes, and (2) can be reformulated as

$$\gamma_X^{\mathrm{r},*} = \gamma_{X,\mathrm{inner}}^{\mathrm{r},0} \gamma_{X,\mathrm{inter}}^{\mathrm{r},0} (1 - \alpha_1(1 - S(f_X^*)))(1 - \alpha_2(1 - S(f_Y^*))), \tag{11}$$

where $S(x)$ is the probability that a node belongs to the giant component (GC) when a random fraction $1 - x$ of the nodes is removed. The model parameters are listed in Appendix A of the Supplementary Material.

III. RESULTS AND ANALYSIS

We construct two multivariate recovery-dependency networks: a homogeneous one comprising two Erdős–Rényi layers (ER–ER) and a heterogeneous one consisting of two scale-free layers (SF–SF), both with one-to-one correspondence coupling. In each case, the two layers are generated using the configuration model [20], with distinct nodes in the two layers connected through one-to-one

correspondence. For ER networks, the degree distribution is $p(k) = \mathrm{e}^{-\langle k\rangle}\frac{\langle k\rangle^k}{k!}$, where $\langle k\rangle$ represents the average degree. For SF networks, the degree distribution is $p(k) = Ck^{-\widetilde{\lambda}}$, where C is the normalization constant, with the distribution typically approximated as $p(k) = (\frac{k_{\min}}{k})^{\widetilde{\lambda}-1} - (\frac{k_{\min}}{k+1})^{\widetilde{\lambda}-1}$, where the minimum degree is $k_{\min}$, and $\widetilde{\lambda}$ denotes the power-law exponent. The numerical simulations are performed independently, each on a newly generated random network according to the prescribed network model and parameters, with no correlation between different simulation runs. Our theoretical results are based on (10) and (11). To describe subsequent random failures, we assume that the number of failures follows an exponential distribution [50, 51]. The exponential distribution is adopted as a simple nonnegative distribution for modeling random failures while maintaining analytical tractability. The probability density is $q(x) = \lambda \mathrm{e}^{-\lambda x}$ $(x > 0)$, where λ is the rate parameter. We first present results for $\tau = 0$, and then discuss the case $\tau > 0$ in the final part of this section.

A. Understanding failure-recovery dynamics

We initially focus on the dynamic recovery evolution of interdependent networks. Figures 2(a) and (b) show the fraction of functional nodes f_X as a function of time t for different families of coupled networks, including homogeneous and heterogeneous ones. Upon reaching equilibrium $(t \to \infty)$, the system stabilizes into one of two distinct states, with the curves either converging toward a functional recovery state $(f_X^* \to 1)$ or descending to a fully collapsed state $(f_X^* = 0)$. The disparities in outcomes are mainly determined by the intensity of the initial attack. Surprisingly, identical initial attack fractions p can lead to system bifurcations across different independent simulation realizations. For example, in the ER–ER network shown in Figure 2(a), when $p = 0.715$, identical parameters yield divergent trajectories, illustrating this behavior. A similar phenomenon is observed in the SF–SF network at $p = 0.72$, as shown in Figure 2(b).

Figures 2(a) and (b) also indicate that each simulation realization eventually reaches a final steady state, corresponding to either successful recovery or system collapse. For a successfully recovered realization, the recovery time is defined as the time at which the system first reaches the recovered steady state. Figures 2(c) and (d) show the mean recovery time T_{RS}, obtained by averaging the recovery times over the successfully recovered realizations from 1,000 independent numerical simulations. Similarly, for realizations ending in system collapse, we define the mean failure time T_{RF}, with both T_{RS} and T_{RF} calculated as described in Appendix D of the Supplementary Material. Clearly, under repeated simulations, three scenarios can be observed for different

values of p: some never result in network failure, some invariably result in failure, and some exhibit uncertain outcomes. Accordingly, we define three regions of behavior: *fully recoverable*, *unrecoverable*, and *partially recoverable*. In the *fully recoverable* region, the network rapidly returns to a fully functional state, which manifests as a critical window for implementing effective rescue measures. In contrast, the *unrecoverable* region corresponds to scenarios where recovery is unattainable, and the time to recovery can be regarded as tending toward infinity. The *partially recoverable* region, exemplified by $p = 0.715$ in Figure 2(a), represents an intermediate phase where the evolutionary outcome is uncertain, and even if the network eventually returns to a fully functional state, the average repair period still increases and tends toward infinity as the initial attack p grows.

To further analyze the causes of these three regions, we study the recovery probability of the network for different network sizes and the corresponding fraction of functional nodes. Figures 3(a) and (c) capture the probability of recovery success, P_{RS}, obtained after multiple independent iterations. Here, we denote the critical points where P_{RS} transitions from one to less than one as p_{c_1}, and from greater than zero to zero as p_{c_2}. In fact, the three regions mentioned in Figures 2(c) and (d) are defined by these two critical points. When the network size is $N = 5 \times 10^4$, the *partially recoverable* region can be clearly observed; however, as N increases, this region becomes increasingly compressed. Clearly, p_{c_1} increases with the growth of network size N, moving closer to p_{c_2}. Physically, p_{c_1} marks the boundary at which the system begins to lose guaranteed recovery, whereas p_{c_2} marks the boundary beyond which recovery is no longer possible. Between the two thresholds, recovery is no longer guaranteed, although the system still retains the ability to recover. This indicates that the size of the network has a significant impact on the system's ability to recover, with larger networks being more resilient to attacks. Figure 3(b) further supports this conclusion, showing that the fraction of functional nodes in the ER–ER network, $\overline{f_X^*}$, which is obtained by directly averaging f_X^*, follows a similar trend to P_{RS}. We observe that $\overline{f_X^*}$ remains consistently below 1 as a result of persistent random failures γ_μ^{d}. In Figures 3(c) and (d), we extend the analysis to SF–SF networks. The results reveal behavior consistent with that of the ER–ER network, exhibiting two critical thresholds, p_{c_1} and p_{c_2}. Specifically, p_{c_1} increases with the network size, whereas p_{c_2} remains relatively stable, independent of N.

B. Exploring scaling laws in recovery dynamics

We further investigate the variation of p_{c_1} as a function of network size N, revealing an interesting scaling relation closely tied to scale invariance. Figure 4(a) shows how the distance between

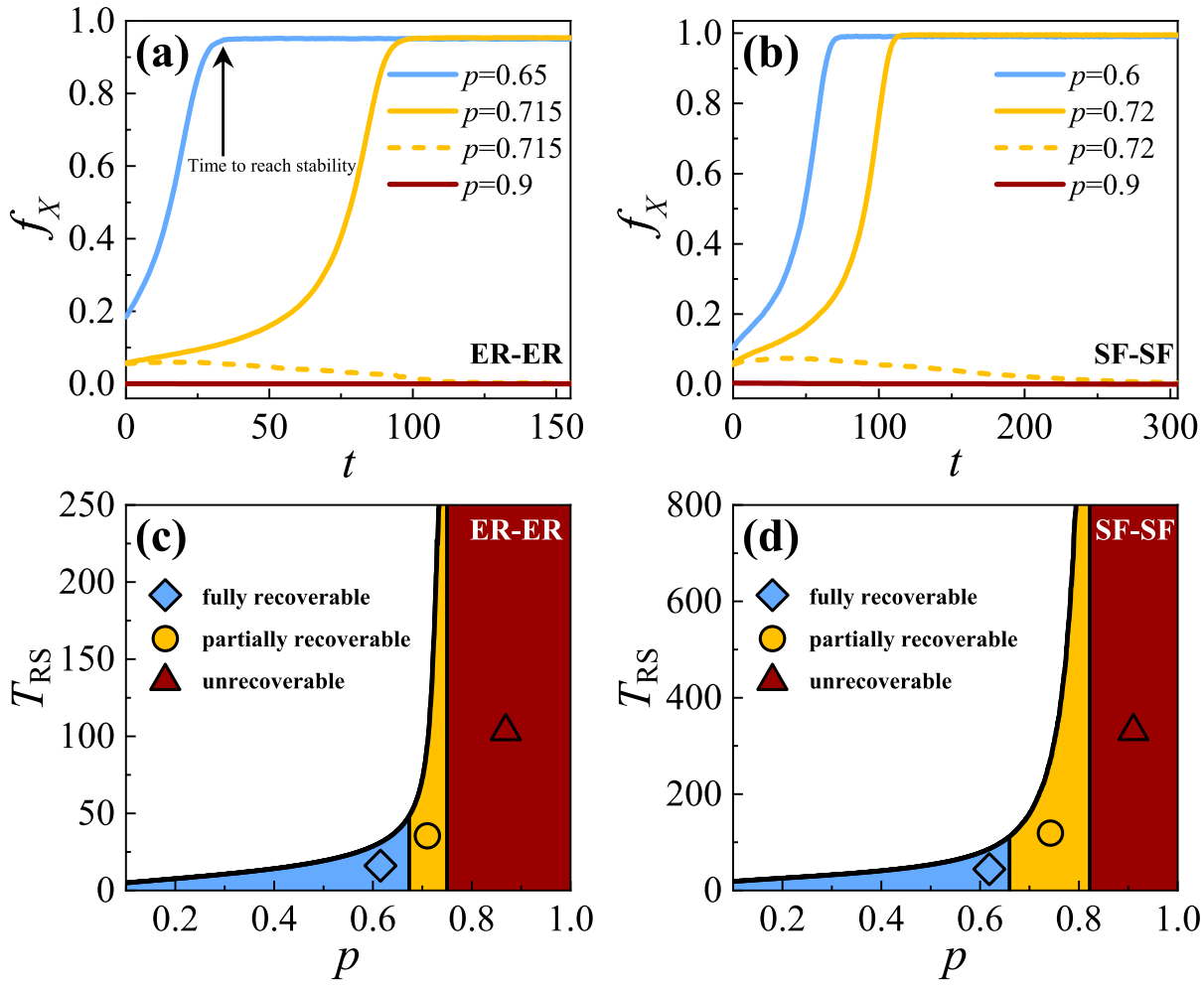

FIG. 2: The fraction of functional nodes in network X, f_X, is shown as a function of time step t, with parameters $N = 50{,}000$, $\gamma^{\mathrm{r},0}_{X,\mathrm{inner}} = \gamma^{\mathrm{r},0}_{X,\mathrm{inter}} = 0.8$, $\alpha_1 = \alpha_2 = 1$, and random failures modeled using an exponential distribution with $\lambda = 0.01$. (a) ER–ER network with $\langle k \rangle = 4$. The system exhibits potential for either recovery ($f^*_X \to 1$) or collapse ($f^*_X = 0$) as $t \to \infty$, depending on the initial attack fraction p. Notably, at $p = 0.715$, the evolution outcomes diverge significantly due to different simulation realizations. (b) SF–SF network with $\widetilde{\lambda} = 3$, $k_{\min} = 2$. Similar to the ER–ER network, the SF–SF network exhibits a bifurcation in the evolution outcomes at $p = 0.72$. (c) and (d) The average recovery time T_{RS} required for the network to reach the functional state. The regions of *fully recoverable* and *unrecoverable* represent ranges in which the system either fully recovers or collapses, and the *partially recoverable* region indicates a transitional state where the system's outcome is uncertain, leading to variability in recovery times.

the two critical points, p_{c_1} and p_{c_2}, changes with network size in the ER–ER network. This relationship exhibits clear scaling behavior, with the scaling exponent γ gradually decreasing alongside the network's average degree $\langle k \rangle$. This indicates that as the network becomes more connected, it exhibits pronounced scaling properties, accompanied by enhanced resilience to failures. As shown

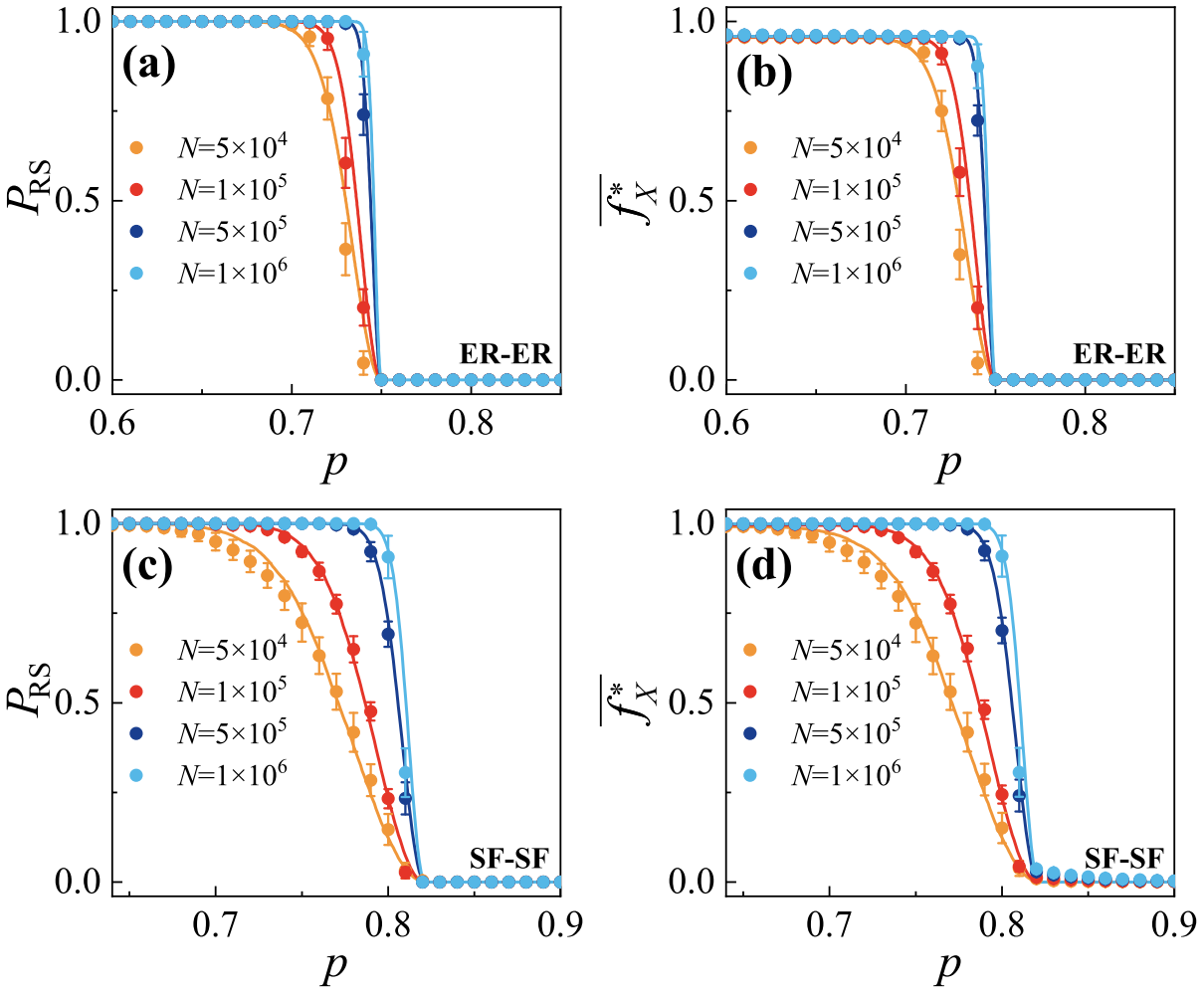

FIG. 3: The probability of recovery success, P_{RS}, and the fraction of functional nodes, $\overline{f_X^*}$, vary with the initial attack fraction p for different network sizes N. (a) and (b) Under the ER–ER network with $\langle k\rangle = 4$, $\gamma_{X,\mathrm{inner}}^{\mathrm{r},0} = \gamma_{X,\mathrm{inter}}^{\mathrm{r},0} = 0.8$, $\alpha_1 = \alpha_2 = 1$, and $\lambda = 0.01$. (c) and (d) Under the SF–SF network with $\widetilde{\lambda} = 3$ and $k_{\min} = 2$. Theoretical predictions (solid lines), based on (10) and (11), are obtained from 10,000 iterations. Simulation results (symbols) are obtained from 1,000 independent realizations, with error bars representing the standard deviation.

in Figure 4(b), the scaling exponent γ decreases with the rise of the power-law exponent $\widetilde{\lambda}$. The decrease of $|p_{\mathrm{c}_1} - p_{\mathrm{c}_2}|$ with increasing N quantitatively shows that the *partially recoverable* region becomes narrower as the system size increases. Since p_{c_2} remains relatively stable with respect to N, this scaling mainly reflects the convergence of p_{c_1} toward p_{c_2}, with network resilience increasing as the system size grows. Figures 4(c) and (d) display the relationship between the probability of recovery failure, $1 - P_{\mathrm{RS}}$, and network size N for a fixed initial attack fraction p. The results follow an exponential decay pattern, with the relationship given by $1 - P_{\mathrm{RS}} = c\mathrm{e}^{-N/N^*}$, where N^* serves

as a fitting parameter. Further analysis in Figure 4(e) reveals a scaling relationship between N^* and the distance between p and p_{c_2}, suggesting that networks with higher connectivity recover more efficiently. For ER–ER networks with varying average degrees, the scaling exponent κ decreases as the average degree $\langle k \rangle$ increases. Similarly, in the SF–SF network shown in Figure 4(f), the scaling exponent κ increases as the power-law exponent $\widetilde{\lambda}$ increases, indicating that as the network becomes more homogeneous, recovery dynamics become slower and more sensitive to changes in connectivity.

C. Threshold behavior of network stability

The critical thresholds p_{c_1} and p_{c_2} define the boundaries between distinct phases in the system's recovery dynamics. These thresholds exhibit similar scaling behavior across different network topologies. Although p_{c_1} depends on network size and gradually converges to p_{c_2} as the network grows, p_{c_2} remains relatively stable with respect to N. This stability in p_{c_2} underscores its role as the critical point beyond which recovery is impossible. To more clearly illustrate the effects of failure on p_{c_2}, we define the control parameter as $d = \gamma_\mu^{\mathrm{d}}$. Figures 5(a) and (b) show the relationship between the critical point p_{c_2} and network structural parameters, such as the average degree $\langle k \rangle$ and the power-law exponent $\widetilde{\lambda}$. In the ER–ER network, p_{c_2} increases sharply as $\langle k \rangle$ increases, and exhibits a distinct jump transition, which suggests that higher connectivity enhances network resilience. Additionally, the critical threshold point p_{c_2} is influenced by the damage rate d. It can be observed that the network's resilience decreases as the damage rate d increases. A similar phenomenon occurs in the SF–SF network, as shown in Figure 5(b). Notably, in the ER–ER network, a higher average degree leads to greater resilience, whereas in the SF–SF network, a smaller power-law exponent $\widetilde{\lambda}$ results in greater resilience. This difference arises because, as the power-law exponent increases, the network becomes more homogeneous. During this transition, the network's average degree tends toward the minimum degree. Since the minimum degree in our SF–SF network is $k_{\min} = 2$, the average degree decreases with increasing power-law exponent, which explains why a smaller power-law exponent corresponds to greater network resilience. These results indicate that p_{c_2} represents the upper limit of system recoverability under a given network structure and damage condition. Once the initial damage exceeds this threshold, the remaining functional connectivity and recovery support are insufficient to restore the network.

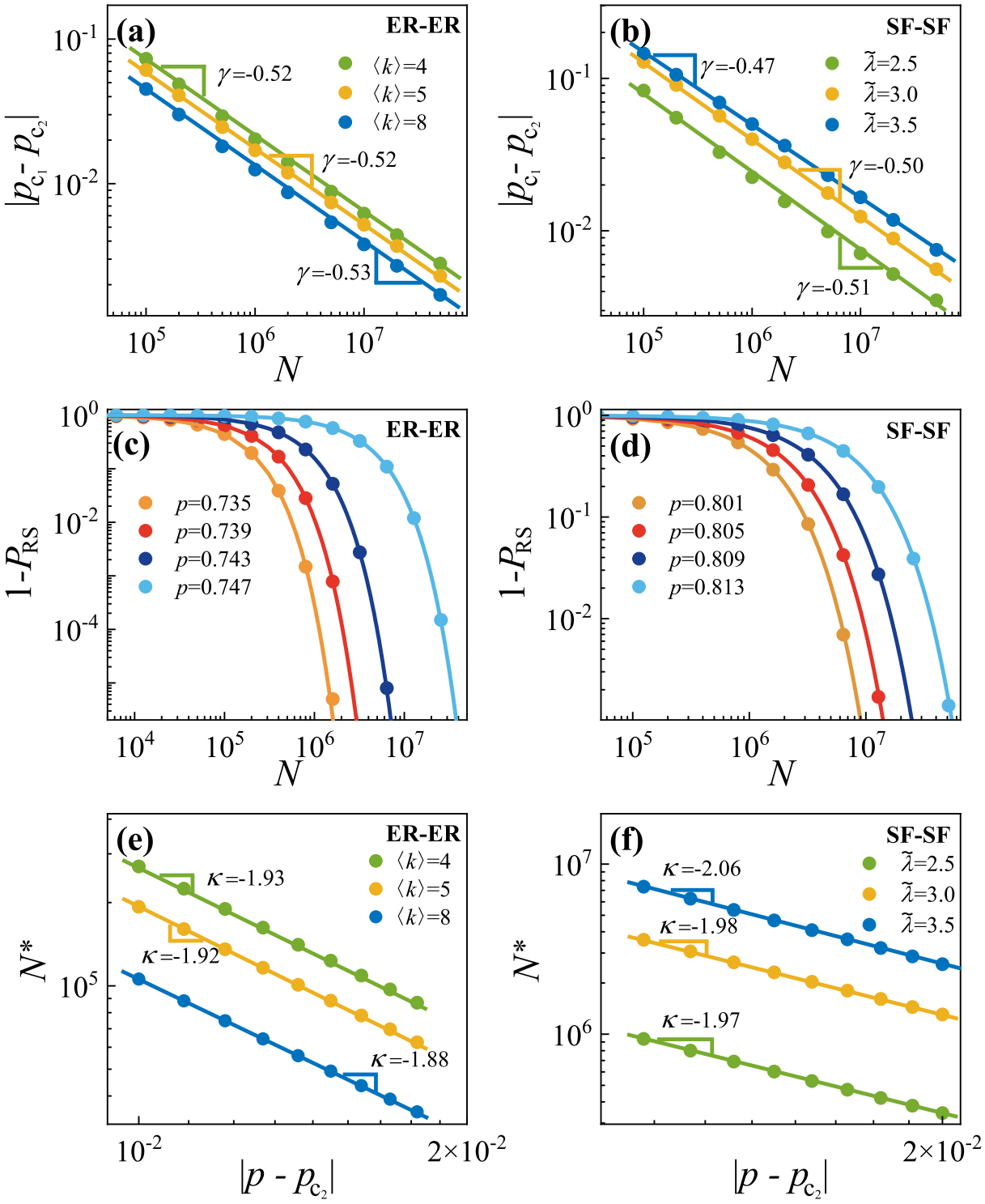

FIG. 4: Critical scaling relationships and exponents for ER–ER and SF–SF networks with varying network sizes N. $|p_{c_1} - p_{c_2}|$ as a function of N. (a) The ER–ER network with $\langle k\rangle = 4$, $\langle k\rangle = 5$, and $\langle k\rangle = 8$. (b) The SF–SF network with $\widetilde{\lambda} = 2.5$, $\widetilde{\lambda} = 3$, and $\widetilde{\lambda} = 3.5$. (c) and (d) $1 - P_{\rm RS}$ as a function of N under different initial failure fractions p. The solid lines represent fitted curves, $1 - P_{\rm RS} = ce^{-N/N^*}$, where N^* is a fitting parameter for the ER–ER network with $\langle k\rangle = 4$ and the SF–SF network with $\widetilde{\lambda} = 3$, respectively. (e) and (f) N^* as a function of $|p - p_{c_2}|$ for both ER–ER and SF–SF networks.

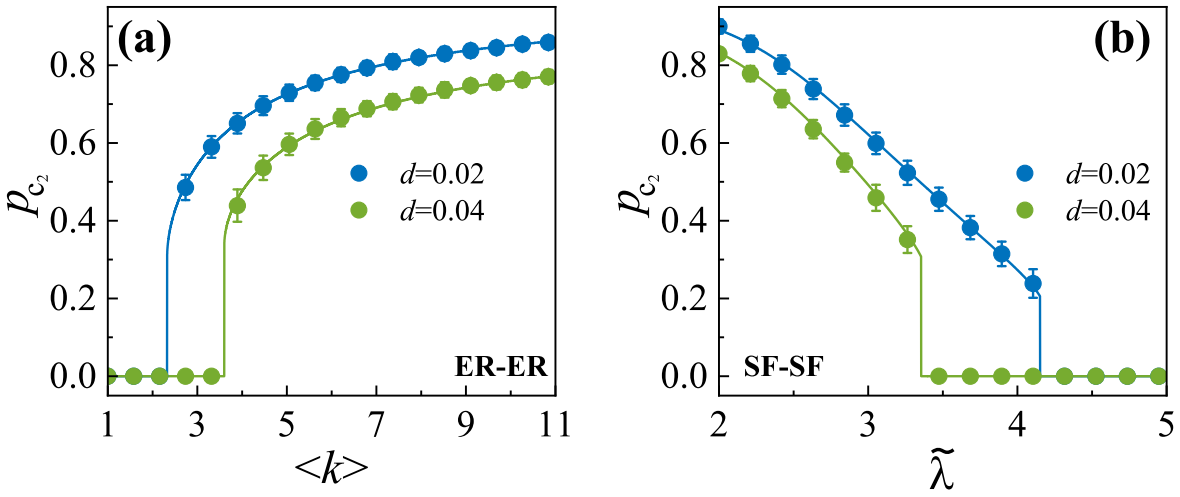

FIG. 5: (a) and (b) Critical points p_{c_2} as a function of different parameters for the ER–ER and SF–SF networks with $N = 50{,}000$, $\gamma^{r,0}_{X,\text{inner}} = \gamma^{r,0}_{X,\text{inter}} = 0.8$, and $\alpha_1 = \alpha_2 = 1$. It is found that when the network's average degree and heterogeneity change, the stability of p_{c_2} is disrupted, exhibiting characteristics of a jump transition.

D. Influence of time delay on recovery processes

In the previous sections, we studied the immediate intervention in the repair process after the network undergoes an initial attack specifically at $\tau = 0$. However, time delays are inherent in real-world recovery processes, arising from logistical challenges, resource shortages, or delayed access to failed nodes. In this context, we analyze the case of $\tau > 0$, which significantly affects the network's ability to recover and alters the overall recovery dynamics. Figures 6(a) and (b) compare the average time required for network recovery T_{RS} under different values of τ in ER–ER and SF–SF networks, respectively. The results reveal that the later the intervention in the recovery process, the higher the T_{RS} value becomes, indicating a longer recovery time. Delayed recovery interventions lead to significant increases in the time required for the network to return to a functional state. Figures 6(c) and (d) show how the probability of recovery success, P_{RS}, is related to the initial attack fraction p. As τ increases, we observe a gradual decrease in the value of P_{RS}. This suggests that the longer the delay before recovery begins, the lower the likelihood of a successful network recovery. In other words, the critical threshold p_{c_1} is influenced not only by the network size N but also decreases with an increase in the intervention time τ. However, within the parameter range considered here, p_{c_2} remains approximately unchanged as τ varies. Furthermore, we analyze the relationship between the distance between two critical points p_{c_1} and p_{c_2} and the intervention repair time τ in the ER–ER and SF–SF networks. The results in Figures 6(e) and (f) indicate a

clear linear relationship between the distance $|p_{c_1} - p_{c_2}|$ and the intervention time τ across different network sizes. As τ increases, the gap between the two critical thresholds widens. However, this gap gradually decreases as the network size increases. In other words, while the distance $|p_{c_1} - p_{c_2}|$ is a linear function of τ, its slope decreases with increasing network size, underscoring the influence of network size on p_{c_1}, consistent with the previous findings. The findings highlight the importance of prompt recovery interventions. Delays in addressing system failures not only increase the time required for recovery but also reduce the probability of restoring full network functionality.

IV. DISCUSSION

This study provides new insights into the recovery dynamics of interdependent networks, focusing on the impact of network topology on recovery behavior and the critical role of time delay. Through the analysis of both homogeneous and heterogeneous networks, we show that the recovery process can be enhanced not only by strengthening critical external support but also by addressing internal influences.

One key finding is that the recovery behavior of the system is characterized by two critical thresholds, p_{c_1} and p_{c_2}, which define the *fully recoverable*, *partially recoverable*, and *unrecoverable* regimes. The existence of these two thresholds indicates that, between the fully recoverable and unrecoverable regimes, there is an intermediate region in which recovery remains possible but is no longer guaranteed. Network size significantly affects the relationship between the two critical thresholds. As network size increases, the gap between p_{c_1} and p_{c_2} decreases, and the *partially recoverable* region gradually narrows. This observation aligns with previous findings that larger networks tend to exhibit greater overall resilience, particularly under continuous failures. Physically, p_{c_1} marks the boundary at which the system begins to lose guaranteed recovery, beyond which different stochastic realizations under the same conditions may lead to different recovery outcomes, whereas p_{c_2} represents the upper limit of system recoverability, beyond which recovery is no longer possible. Moreover, the scaling behaviors identified in the recovery dynamics are also observed in stochastic block model (SBM) networks and spatial hyperbolic networks, providing further support for their generality across different network topologies; see Appendix E of the Supplementary Material.

Another important conclusion is that increasing the time delay directly affects the recovery process by extending the time required for the network to stabilize, as shown by the increase in T_{RS}. Delays in intervention not only prolong the recovery duration but also reduce the overall

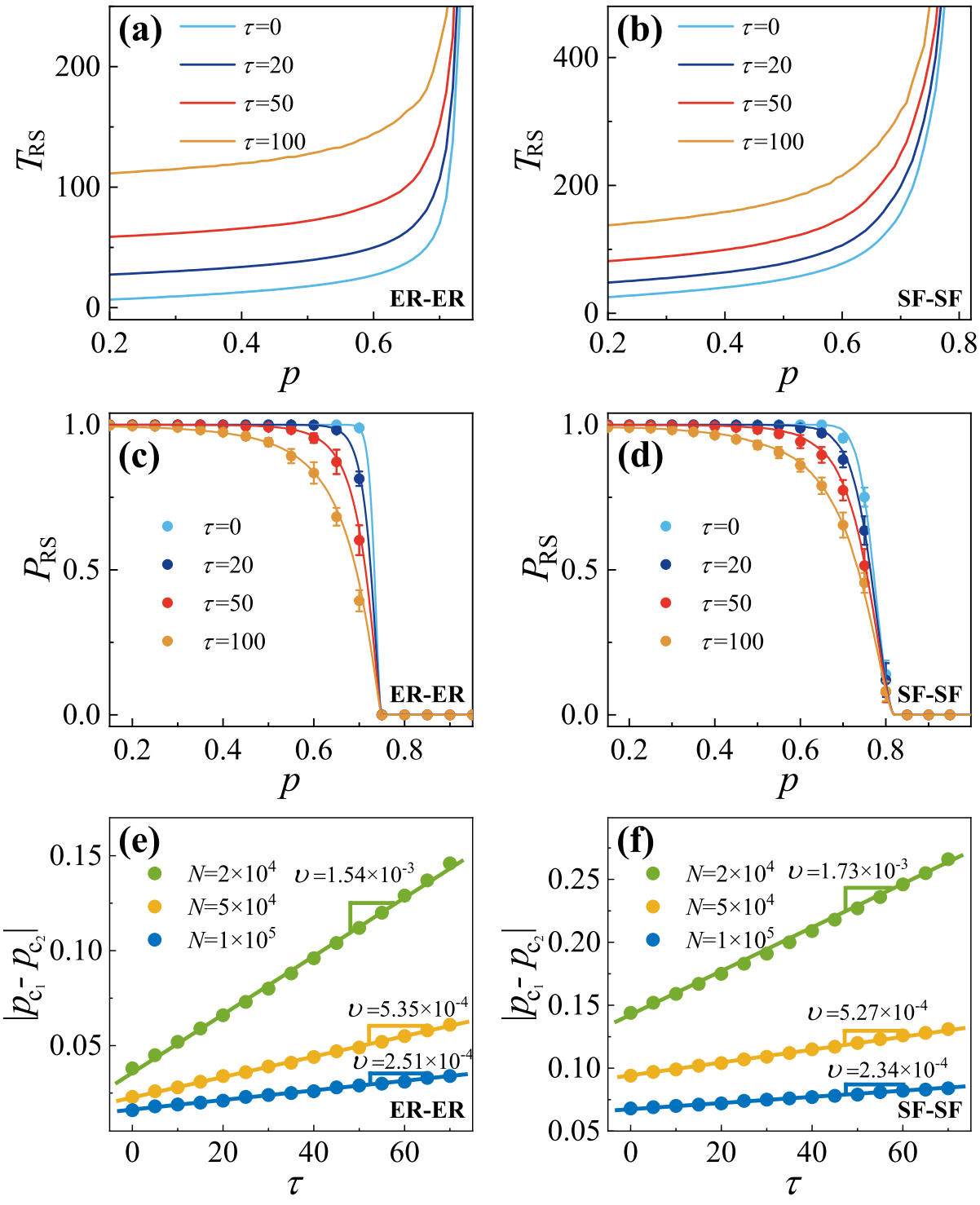

FIG. 6: The average time required $T_{\rm RS}$ as a function of the initial attack fraction p for different time delays τ in (a) the ER–ER network with $\langle k\rangle = 4$ and (b) the SF–SF network with $\widetilde{\lambda} = 3$. The other parameters are $N = 50{,}000$, $\gamma^{\rm r,0}_{X,\rm inner} = \gamma^{\rm r,0}_{X,\rm inter} = 0.8$, $\alpha_1 = \alpha_2 = 1$ and $\lambda = 0.01$. (c) and (d) The probability of recovery success $P_{\rm RS}$ as a function of p for different τ in the ER–ER and SF–SF networks, respectively. Simulation results (symbols) are averaged over 1,000 realizations, with error bars representing the standard deviation, and are consistent with the theoretical results (solid lines). (e) and (f) $|p_{c_1} - p_{c_2}|$ as a function of τ for different N.

probability of recovery success P_{RS}, as demonstrated in both the ER–ER and SF–SF networks. This relationship between τ and P_{RS} suggests that recovery delays weaken the network's recuperative capacity, particularly when faced with large-scale failures.

Network topology significantly influences recovery dynamics. Different network structures exhibit distinct recovery behaviors and varying sensitivities to time delays. This underscores the importance of considering network topology when designing recovery strategies, as the effectiveness of recovery interventions may vary depending on the underlying structure of the network. At the same time, the current model adopts several simplifying assumptions, including one-to-one inter-layer dependency and a uniform effective recovery delay. Future work may further consider heterogeneous inter-layer dependency patterns, node-dependent recovery delays, and non-uniform recovery resources to better characterize recovery processes in real interdependent systems.

In practical infrastructure applications, the proposed framework can be further connected with measurable system data. Infrastructure information, geographic information system (GIS) data, and operational records can be used to construct the network layers and their inter-layer dependencies, while component-status, failure, and restoration records can be used to estimate the recovery-related parameters and the effective recovery delay τ. After model calibration, repeated simulations on the observed network under damage scenarios with varying initial damage fractions p can be performed to estimate the recovery success probability $P_{\mathrm{RS}}(p)$. The two critical thresholds can then be identified as transition ranges in $P_{\mathrm{RS}}(p)$, with uncertainty evaluated according to the available data, number of simulations, and selected recovery criteria. Therefore, these thresholds should be regarded as model-based estimates conditional on specific system conditions, damage scenarios, and modeling assumptions, rather than exact values directly observable from a single event.

In summary, our analysis demonstrates that timely recovery interventions are critical for maintaining network resilience. Delays in recovery not only extend the time required for stabilization but also reduce the likelihood of full recovery. While larger networks can mitigate the negative effects of delays, the coupled recovery dependency makes system recovery jointly constrained by intra-layer and inter-layer support, and insufficient support from either pathway may hinder recovery. These findings provide valuable insights for designing more robust interdependent networks, with implications for real-world systems such as power grids, communication networks, and transportation systems.

Acknowledgements

This work was supported by the National Natural Science Foundation of China (Grant Nos. 72474086, 62373169, 12526638 and 62603349), the National Statistical Science Research Project (Grant No. 2025LZ005), the Basic Research Program of Jiangsu (Grant No. BK20250637), the Jiangsu Provincial University Natural Science Research General Program (Grant No. 25KJB120006), the Ministry of Education Key Laboratory of NSLSCS (Grant No. 181070H602), the Young and Mid-career Academic Leader of the Jiangsu Province Qinglan Project in 2024, and the Postgraduate Research & Practice Innovation Program of Jiangsu Province (Grant No. 26CXJH7072). R. L. acknowledges support from Engineering and Physical Sciences Research Council (Grant Nos. EP/V013068/1, EP/V03474X/1, EP/Y028872/1) and International Exchanges IEC\NSFC\201180 of the Royal Society.

References

[1] Gao J X, Barzel B, Barabási A L. Universal resilience patterns in complex networks. Nature, 2016, 530: 307–312

[2] Liu C, Xu F L, Gao C, et al. Deep learning resilience inference for complex networked systems. Nat Commun, 2024, 15: 9203

[3] De Domenico M. More is different in real-world multilayer networks. Nat Phys, 2023, 19: 1247–1262

[4] Dong G G, Wang F, Shekhtman L M, et al. Optimal resilience of modular interacting networks. Proc Natl Acad Sci USA, 2021, 118: e1922831118

[5] Li Q, Yu H T, Han W T, et al. Robustness of interdependent networks with weak dependency links and reinforced nodes. Sci China Inf Sci, 2024, 67: 129201

[6] Pan X Y, Zhou J, Zhou Y Z, et al. Robustness of interdependent hypergraphs: a bipartite network framework. Phys Rev Res, 2024, 6: 013049

[7] Artime O, Grassia M, De Domenico M, et al. Robustness and resilience of complex networks. Nat Rev Phys, 2024, 6: 114–131

[8] Kilanitis I, Sextos A. Integrated seismic risk and resilience assessment of roadway networks in earthquake prone areas. Bull Earthquake Eng, 2019, 17: 181–210

[9] Espinoza S, Poulos A, Rudnick H, et al. Risk and resilience assessment with component criticality ranking of electric power systems subject to earthquakes. IEEE Syst J, 2020, 14: 2837–2848

[10] Hu X Q, Dong G G, Christensen K, et al. Unveiling the importance of nonshortest paths in quantum networks. Sci Adv, 2025, 11: eadt2404

[11] Ren G D, Meng T Z, Ma Y. Sugars altered fungal community composition and caused high network

complexity in a Fusarium wilt pathogen-infested soil. Biol Fertil Soils, 2020, 56: 395–409

[12] Yang Y, Nishikawa T, Motter A E. Small vulnerable sets determine large network cascades in power grids. Science, 2017, 358: eaan3184

[13] Abedi A, Gaudard L, Romerio F. Review of major approaches to analyze vulnerability in power system. Reliab Eng Syst Saf, 2019, 183: 153–172

[14] Yabe T, Rao P S C, Ukkusuri S V, et al. Toward data-driven, dynamical complex systems approaches to disaster resilience. Proc Natl Acad Sci USA, 2022, 119: e2111997119

[15] Kruczkiewicz A, Klopp J, Fisher J, et al. Compound risks and complex emergencies require new approaches to preparedness. Proc Natl Acad Sci USA, 2021, 118: e2106795118

[16] Zhai C, Xiao G X, Zhang H H, et al. Identifying disruptive contingencies for catastrophic cascading failures in power systems. Int J Electr Power Energy Syst, 2020, 123: 106214

[17] Feng K R, Ouyang M, Lin N. Tropical cyclone-blackout-heatwave compound hazard resilience in a changing climate. Nat Commun, 2022, 13: 4421

[18] Cimellaro G P, Crupi P, Kim H U, et al. Modeling interdependencies of critical infrastructures after Hurricane Sandy. Int J Disaster Risk Reduct, 2019, 38: 101191

[19] Buldyrev S V, Parshani R, Paul G, et al. Catastrophic cascade of failures in interdependent networks. Nature, 2010, 464: 1025–1028

[20] Shao J, Buldyrev S V, Havlin S, et al. Cascade of failures in coupled network systems with multiple support-dependence relations. Phys Rev E, 2011, 83: 036116

[21] Parshani R, Buldyrev S V, Havlin S. Critical effect of dependency groups on the function of networks. Proc Natl Acad Sci USA, 2011, 108: 1007–1010

[22] Meng X Y, Zhu C X G, Pedreschi N, et al. Unifying network connectivity from geodesics to random walks via the random cluster model. Nat Commun, 2026, 17: 8187

[23] Kuzyk Z Z A, Leblanc M, Ehn J, et al. Eelgrass ecosystem collapse and social-ecological regime shift driven by hydropower development and climate change. Nat Commun, 2026, 17: 2917

[24] Lee U, Kim H, Kim M, et al. Proximity to explosive synchronization determines network collapse and recovery trajectories in neural and economic crises. Proc Natl Acad Sci USA, 2025, 122: e2505434122

[25] D'Souza R M, di Bernardo M, Liu Y Y. Controlling complex networks with complex nodes. Nat Rev Phys, 2023, 5: 250–262

[26] Kaiser F, Latora V, Witthaut D. Network isolators inhibit failure spreading in complex networks. Nat Commun, 2021, 12: 3143

[27] Dong C, Xiong X X, Xue Q L, et al. A survey on the network models applied in the industrial network optimization. Sci China Inf Sci, 2024, 67: 121301

[28] Sanhedrai H, Havlin S. Sustaining a network by controlling a fraction of nodes. Commun Phys, 2023, 6: 22

[29] Pang Y Y, Li H, Tang P, et al. Synchronization optimization of pipe diameter and operation frequency in a pressurized irrigation network based on the genetic algorithm. Agriculture, 2022, 12: 673

[30] Sun W M, Zeng A. Target recovery in complex networks. Eur Phys J B, 2017, 90: 10

[31] Jiang Y, Yan Y W, Hong C, et al. Multidirectional recovery strategy against failure. Chaos Solitons Fractals, 2022, 160: 112272

[32] La Rocca C E, Stanley H E, Braunstein L A. Strategy for stopping failure cascades in interdependent networks. Phys A-Stat Mech Appl, 2018, 508: 577–583

[33] Majdandzic A, Podobnik B, Buldyrev S V, et al. Spontaneous recovery in dynamical networks. Nat Phys, 2014, 10: 34–38

[34] Tachaudomdach S, Upayokin A, Kronprasert N, et al. Quantifying road-network robustness toward flood-resilient transportation systems. Sustainability, 2021, 13: 3172

[35] Lhomme S, Serre D, Diab Y, et al. Analyzing resilience of urban networks: a preliminary step towards more flood resilient cities. Nat Hazards Earth Syst Sci, 2013, 13: 221–230

[36] Sharkey T C, Nurre S G, Nguyen H, et al. Identification and classification of restoration interdependencies in the wake of Hurricane Sandy. J Infrastruct Syst, 2016, 22: 04015007

[37] Liu X M, Yan X, Stanley H E. Spontaneous recovery in directed dynamical networks. Engineering, 2024, 37: 208–214

[38] Peng H, Kuang Z H, Zhao D D, et al. Spontaneous recovery in random hypergraphs. Chaos, 2024, 34: 073113

[39] Daniotti S, Servedio V D P, Kager J, et al. Systemic risk approach to mitigate delay cascading in railway networks. npj Sustain Mobil Transp, 2024, 1: 15

[40] Danziger M M, Barabási A L. Recovery coupling in multilayer networks. Nat Commun, 2022, 13: 955

[41] Zhang W X, Han Q, Shang W L, et al. Seismic resilience assessment of interdependent urban transportation-electric power system under uncertainty. Transp Res Part A-Policy Pract, 2024, 183: 104078

[42] Wang W, He Y F, Wang H B, et al. Improving interdependent urban power and gas distribution systems resilience through optimal scheduling of mobile emergency supply and repair resources. Reliab Eng Syst Saf, 2024, 250: 110303

[43] Yanchuk S, Giacomelli G. Spatio-temporal phenomena in complex systems with time delays. J Phys A-Math Theor, 2017, 50: 103001

[44] Yang Y G, Foster K R, Coyte K Z, et al. Time delays modulate the stability of complex ecosystems. Nat Ecol Evol, 2023, 7: 1610–1619

[45] Zhao G D, Song R R, Zhang H J. Optimal control of smart grids based on weighted network congestion games with time delay via state-flipped control. Sci China Inf Sci, 2026, 69: 140214

[46] Rehak D, Senovsky P, Slivkova S. Resilience of critical infrastructure elements and its main factors. Systems, 2018, 6: 21

[47] Zhang J H, Liu H Y, Yu G D, et al. A three-stage and multi-objective stochastic programming model to improve the sustainable rescue ability by considering secondary disasters in emergency logistics. Comput Ind Eng, 2019, 135: 1145–1154

[48] Feng L, Monterola C P, Hu Y Q. The simplified self-consistent probabilities method for percolation and its application to interdependent networks. New J Phys, 2015, 17: 063025

[49] Dong G G, Luo Y T, Liu Y Y, et al. Percolation behaviors of a network of networks under intentional attack with limited information. Chaos Solitons Fractals, 2022, 159: 112147

[50] Liu Y M, Sui S B, Lu D, et al. Emergent lifetime distribution from complex network systems aging. Reliab Eng Syst Saf, 2024, 247: 110128

[51] Collins D H, Warr R L. Failure time distributions for complex equipment. Qual Reliab Eng Int, 2019, 35: 146–154

Supplementary Files

This is a list of supplementary files associated with this preprint. Click to download.

- SupplementaryMaterial.pdf